Chinese Chemical Letters 33 (2022) 217–220

Contents lists available at ScienceDirect

Chinese Chemical Letters

journal homepage: www.elsevier.com/locate/cclet

Synthesis, characterization and reactivity of thiolate-bridged cobalt-iron and ruthenium-iron complexes

Chao Guo[a], Linan Su[a,*], Dawei Yang[a], Baomin Wang[a], Jingping Qu[a,b]

[a] State Key Laboratory of Fine Chemicals, Dalian University of Technology, Dalian 116024, China
[b] State Key Laboratory of Bioreactor Engineering, Shanghai Collaborative Innovation Centre for Biomanufacturing, Frontiers Science Center for Materiobiology and Dynamic Chemistry, East China University of Science and Technology, Shanghai 200237, China

ARTICLE INFO

Article history:
Received 22 April 2021
Revised 22 June 2021
Accepted 25 June 2021
Available online 3 July 2021

Keywords:
Metallic cooperativity
Heterobinuclear complex
Hydrazine disproportionation
Metallothiolate ligand
Metal-sulfur cluster

ABSTRACT

Thiolate-bridged hetero-bimetallic complexes $[Cp^*M(MeCN)N_2S_2FeCl][PF_6]$ (**2**, M = Ru; **3**, M = Co, Cp^* = η^5-C_5Me_5, N_2S_2 = *N,N'*-dimethyl-3,6-diazanonane-1,8-dithiolate) were prepared by self-assembly of dimer $[N_2S_2Fe]_2$ with mononuclear precursor $[Cp^*Ru(MeCN)_3][PF_6]$ or $[Cp^*Co(MeCN)_3][PF_6]_2$ in the presence of $CHCl_3$ as a chloride donor. Complexes **2** and **3** exhibit obviously different redox behaviors investigated by cyclic voltammetry and spin density distributions supported by DFT calculations. Notably, iron-cobalt complex **3** possesses versatile reactivities that cannot be achieved for complex **2**. In the presence of $CoCp_2$, complex **3** can undergo one-electron reduction to generate a stable formally $Co^{II}Fe^{II}$ complex $[Cp^*CoN_2S_2FeCl]$ (**4**). Besides, the terminal chloride on the iron center in **3** can be removed by dehalogenation agent $AgPF_6$ or exchanged with azide to afford the corresponding complexes $[Cp^*Co(MeCN)N_2S_2Fe(MeCN)][PF_6]_2$ (**5**) and $[Cp^*Co(MeCN)N_2S_2Fe(N_3)][PF_6]$ (**6**). In addition, complexes **2, 3** and **4** show distinct catalytic reactivity toward the disproportionation of hydrazine into ammonia. These results may be helpful to understand the vital role of the heterometal in some catalytic transformations promoted by heteromultinuclear complexes.

The cooperativity of different transition metals is widely adopted in metalloenzymes, such as Mo/V-dependent nitrogenase, [NiFe]-hydrogenase and carbon monoxide dehydrogenase, which employ heteromultinuclear metal-sulfur clusters as their active centers [1-3]. Inspired by these natural synthetic systems, artificial heteromultinuclear catalysts are synthesized and proved to display unique catalytic properties. For these catalysts, different transition metals in close proximity may activate substrates simultaneously or consecutively, while such activation modes are hard to achieve by mononuclear or even homodinuclear complexes [4-8]. Furthermore, incorporating another different metal into a monometallic species is likely to modulate its stability, electrochemical properties and reactivity. Therefore, understanding the mutual influence of different metals assumes great significance in uncovering the mechanism of the abovementioned metalloenzymes and designing efficient catalysts.

Although many heteromultinuclear complexes have been developed for homogeneous catalysis applications [9-16], for example, selective hydroformylation by the Pd/Co mixed catalyst reported by Hidai *et al.* [15] and alkyne silylformylation by the Co/Rh catalyst reported by Nakamura *et al.* [16], the cooperative effect of transition metals is, however, still far from being fully understood at a molecular level until now. From a practical standpoint, heterobinuclear complexes would serve as more ideal models to probe into the influence between two different active sites in catalysts [17-21]. However, the coordination environment of reported heterobinuclear complexes makes it difficult to directly evaluate the cooperativity of metals without considering the impact of auxiliary ligands. Therefore, heterobinuclear complexes with the same coordinated sphere are specially needed.

In our previous work, bimetallic cooperativity was adopted to synthesize a series of thiolate-bridged homo- [22-24] and heterodinuclear complexes [25-29] for small molecule activation and transformation. Recently, we reported the synthesis of a thiolate-bridged homobinuclear complex $[Cp^*Fe(MeCN)N_2S_2FeCl][PF_6]$ (**1**) through the assembly of $[N_2S_2Fe]_2$ (N_2S_2 = *N,N'*-dimethyl-3,6-diazanonane-1,8-dithiolate) [30] and $[Cp^*Fe^{II}(MeCN)_3][PF_6]$ (Cp^* = η^5-C_5Me_5) promoted by C−Cl bond cleavage of $CHCl_3$ [31]. As a further extension of this strategy, $[N_2S_2Fe]_2$ may also serve as a good precursor for the synthesis of heterobinuclear complexes featuring a mononuclear reaction moiety $\{N_2S_2FeCl\}$. Herein, we report the synthesis and characterization of novel thiolate-bridged

* Corresponding author.
E-mail address: lnsu@dlut.edu.cn (L. Su).

https://doi.org/10.1016/j.cclet.2021.06.070
1001-8417/

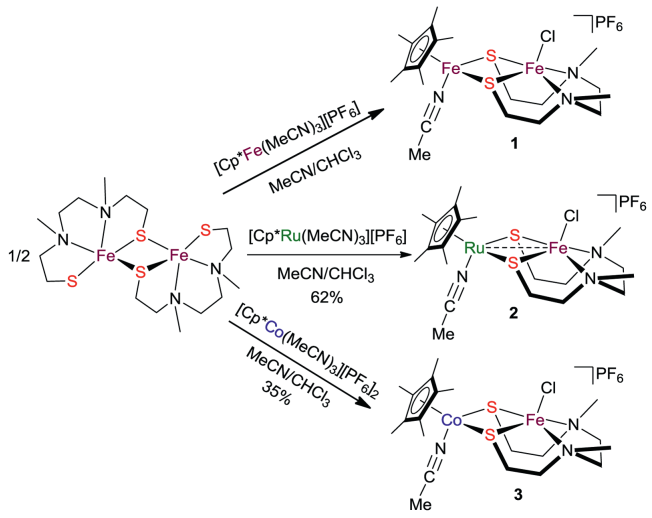

Scheme 1. Synthesis of complexes **1**, **2** and **3**.

iron-ruthenium and iron-cobalt complexes. Experimental results and theoretical analysis reveal the differences in redox properties and spin distributions between the two heterobinuclear complexes, which may have a significant impact on their reactivity.

As outlined in Scheme 1, treatment of the dimeric iron complex $[N_2S_2Fe]_2$ with 2 equiv. of mononuclear ruthenium complex $[Cp^*Ru(MeCN)_3][PF_6]$ [32] in $MeCN/CHCl_3$ (10:1) at room temperature resulted in the dissociation and recombination to generate a thiolate-bridged iron-ruthenium complex $[Cp^*Ru(MeCN)N_2S_2FeCl][PF_6]$ (**2**) in 62% yield as a blue powder. Similarly, thiolate-bridged iron-cobalt complex $[Cp^*Co(MeCN)N_2S_2FeCl][PF_6]$ (**3**) can also be facilely synthesized as a dark red powder by using $[Cp^*Co(MeCN)_3][PF_6]_2$ [33] as the mononuclear precursor. From simple charge balance consideration, the formal oxidation states of the two metallic centers in these two complexes are +2 and +3 valences. However, compared to **2**, the formation of **3** does not need additional oxidant or reductant since the two precursors are in +2 and +3 oxidation states, respectively.

The electrospray ionization high-resolution mass spectrometry (ESI-HRMS) of **2** shows a molecular ion peak at *m/z* 534.0168 (calcd. 534.0169) for $[\mathbf{2}-MeCN-PF_6]^+$. The ESI-HRMS analysis of **3** exhibits a molecular ion peak at *m/z* 491.0456 (calcd. 491.0456) for $[\mathbf{3}-MeCN-PF_6]^+$. The appropriate isotopic distributions confirm the existence of ruthenium and cobalt in **2** and **3**, respectively. The ^1H NMR spectrum of **2** shows two characteristic broad peaks at δ 15.69 and 9.68 ppm, which exhibit obviously strong paramagnetic shift. Differently, the ^1H NMR spectrum of **3** shows only one relatively weak broad peak at δ 0.65 ppm. We preliminarily assign these resonances to the proton signals of the Cp* ligand in **2** and **3**. However, further accurate assignments for these signals are difficult due to their paramagnetism. Subsequently, the magnetic susceptibility measurements of **2** and **3** in solution were conducted by the Evans' method [34]. The values of effective magnetic moments (μ_{eff}) of **2** and **3** are 5.69 and 5.18 μ_B, respectively, which indicate **2** and **3** are in an $S = 5/2$ and 2 ground spin states at room temperature.

Furthermore, complexes **2** and **3** were identified by X-ray crystallographic characterization. The molecular structures of **2** and **3** are shown in Fig. 1 and the main bond lengths and angles are listed in Table 1. Their overall geometric configurations resemble their diiron analogue **1** very closely. Complexes **2** and **3** both possess a distorted square pyramid moiety with the Fe atom embedding in the N_2S_2 plane and the chloride atom locating in the

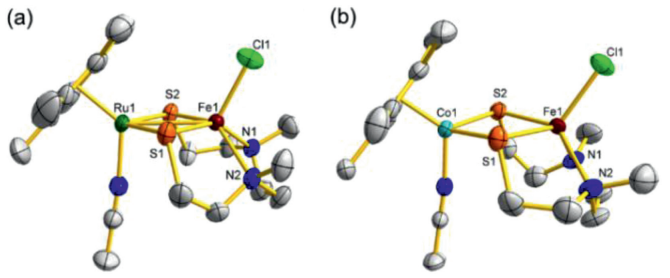

Fig. 1. ORTEP (ellipsoids at 50% probability) diagrams of complexes **2** (a) and **3** (b). All hydrogen atoms and the PF_6^- anion are omitted for clarity.

Table 1
Selected bond lengths [Å] and bond angles [°] of complexes **1, 2** and **3**.

Complex	1	2	3
M1···M2	3.115(1)	2.9883(7)	3.437(3)
Fe1−S1	2.401(2)	2.3821(14)	2.4122(13)
Fe1−S2	2.442(1)	2.3679(13)	2.4537(12)
Fe1−Cl1	2.238(1)	2.2355(14)	2.2561(13)
S1−Fe1−S2	100.61(6)	101.30(5)	82.36(4)
M1−S1−M2	82.89(5)	78.19(4)	94.22(4)
M1−S2−M2	83.38(5)	78.32(4)	93.21(4)

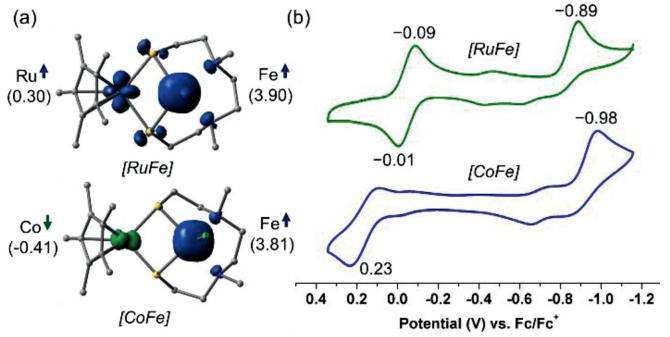

Fig. 2. (a) Spin density analyses of **2** and **3**, spin up is shown in blue, and spin down is shown in green (Isosurface = 0.02). (b) Cyclic voltammograms of **2** (green) and **3** (blue), measured in 0.1 mol/L $^nBu_4NPF_6$ in CH_2Cl_2 at 100 mV/s and internally referenced to Fc^+/Fc.

apical position. Differently, the Ru and Co cores are both in a three-legged piano-stool coordination geometry with one MeCN molecule and two sulfur atoms of the N_2S_2 ligand. Although Ru atom has larger atomic radius than the first row Fe and Co, interestingly, the Ru1···Fe1 distance (2.9883(7) Å) in **2** is significantly shorter than Fe1···Fe2 (3.115(1) Å) in **1** and Fe1···Co1 (3.437(3) Å) in **3**. Additionally, the Ru1···Fe1 distance in **2** is longer than those of other reported thiolate-bridged iron-ruthenium complexes (2.564(1) to 2.691(2) Å) [35-38]. In sharp contrast, the Co1···Fe1 distance in **2** is remarkably longer than those of previously reported thiolate-bridged iron-cobalt complexes (2.398(1) to 2.796(1) Å) [27,28,38-40], even one possessing a similar coordination sphere (3.136 (2) Å) [41]. The obvious difference of bimetallic distance among these complexes may indicate different redox properties and reactivity.

With the molecular structures of these bimetallic complexes as starting points, geometry optimized models were generated from DFT calculation at the TPSSTPSS/LanL2DZ/6–31G(d) level of theory, which indicates **2** and **3** are in an $S = 5/2$ and 2 ground spin states, respectively (Table S8 in Supporting information). The computed key geometric parameters match those determined by X-ray crystallography well, which validate the computational methodology (Tables S9 and S10 in Supporting information). The spin density distribution for complexes **2** and **3** is depicted in Fig. 2a, and it shows a significant amount of spin is located on the Fe1 (spin up)

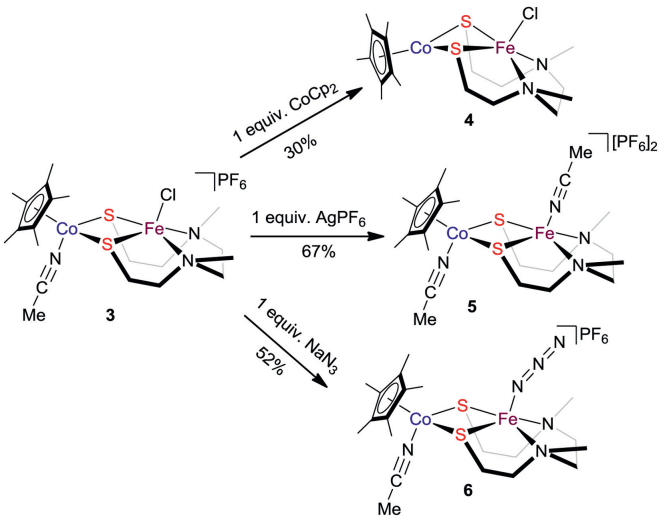

Scheme 2. The reactivity of complex **3**.

of both the two complexes. The similar Mulliken spin populations (3.90 and 3.81) indicate the same +2 oxidation state of Fe1 in **2** and **3**. Based on these results, we assume that the spin state of Fe1 is mainly determined by its coordination configuration and less affected by the other metal core. In addition, a moderate amount of spin is located on the Ru core in **2** (0.30) and the bridging S atoms, while the spin located on the Co core in **3** has the opposite sign (−0.41) and there is barely no spin located on the S atoms in **2**.

The redox behaviors of complexes **2** and **3** were also investigated by cyclic voltammetry in dichloromethane solution (Fig. 2b). According to the cyclic voltammograms of reported bimetallic complexes with similar coordination spheres [42,43], we attribute the first irreversible redox event (green) at reduction peak potential E_{pa} = −0.89 V *vs.* ferrocene $(Fc)^{+/0}$ to the $\{N_2S_2FeCl\}^{II/I}$ redox couple of **2**, which shows a remarkable positive shift of 250 mV compared to that of **1** (E_{pa} = −1.14 V) [31]. The results imply a greater ease of reduction at the $\{N_2S_2FeCl\}$ moiety modulated by the {Cp*Ru} moiety. Likewise, complex **3** also undergoes an irreversible $\{N_2S_2FeCl\}^{II/I}$ reduction event at E_{pa} = −0.98 V (blue), which is only *ca.* 90 mV more negative than that of **2**. The second reversible redox wave of **2** (green) at half-wave potential $E_{1/2}$ = −0.05 V is assigned to the $\{Cp^*Ru\}^{III/II}$ redox couple, which shows a negative shift of 180 mV with respect to that of **1** ($E_{1/2}$ = 0.13 V). Differently, complex **3** shows a quasi-reversible $\{Cp^*Co\}^{III/II}$ oxidation event at E_c = 0.23 V (blue), which probably corresponds to the easy oxidative degradation of the{Cp*Co} moiety.

With the synthesis and characterization of **2** and **3** being achieved, we next investigated the reactivity of the two heterobinuclear complexes. Firstly, we probed into the possibility of their one-electron reduction as predicted by electrochemical studies. Upon interaction of **2** in CH_2Cl_2 with one-electron reductant cobaltocene ($CoCp_2$), insoluble species immediately formed and its poor solubility in common solvents limited further characterization. This experimental fact suggests the reduced product is very unstable and cannot maintain its bimetallic framework. In sharp contrast, one-electron reduction of **3** conducted in similar conditions exhibits completely different reaction phenomenon (Scheme 2). Crystallographic analysis clearly reveals the final product is a neutral formally $Fe^{II}Co^{II}$ complex $[Cp^*CoN_2S_2FeCl]$ (**4**). As shown in Fig. 3a, the acetonitrile ligand is removed after reduction and the Co1···Fe1 distance of 3.109(2) Å is *ca.* 0.33 Å shorter than that of its precursor **3**. The Fe1−Cl1 distance (2.2762(12) Å) in **4** is slightly longer than those of **1** (2.238(1) Å), **2** (2.2355(14) Å) and **3** (2.2561(13) Å),

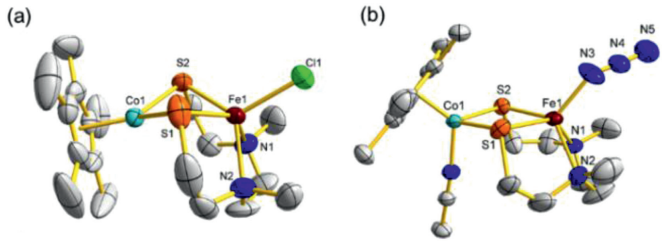

Fig. 3. ORTEP (ellipsoids at 50% probability) diagrams of complexes **4** (a) and **6′** (b). All hydrogen atoms and the BPh_4^- anion of **6′** are omitted for clarity.

which indicates the electron-rich {Cp*Co} moiety may increase the lability of the chloride, thus affecting the reactivity of $\{N_2S_2FeCl\}$ moiety. The ^{1}H NMR spectrum of **4** also reveals its paramagnetic nature and shows a broad singlet at δ −2.17 ppm in the higher field compared with its precursor **3**. The μ_{eff} value of **4** is 5.87 μ_B, indicating **4** is also in an S = 5/2 ground spin state at room temperature.

In order to open the potential reaction site, we next attempted to remove the chloride group. As illustrated in Scheme 2, treatment of **3** with 1 equiv. of $AgPF_6$ in CH_2Cl_2 at room temperature afforded a new heterobinuclear complex $[Cp^*Co(MeCN)N_2S_2Fe(MeCN)][PF_6]_2$ (**5**). The ^{1}H NMR spectroscopic analysis at room temperature shows a broad paramagnetic signal appears at δ −0.87 ppm. In the infrared (IR) spectrum of **5**, a diagnostic weak absorption band at 2283 cm^{-1} is observed, which is attributed to the C≡N stretch vibration of the MeCN ligands. Crystallographic analysis reveals the replacement of the terminal chloride by a MeCN molecule and there are two MeCN ligands separately bound to the Co and Fe centers in a *trans* arrangement (Fig. S4 in Supporting information). The Co1···Fe1 distance of 3.3545(2) Å is only *ca.* 0.08 Å shorter than that of **3**. In addition, two PF_6^- anions are located in the same unit cell, which confirms complex **5** is a dicationic species. Unfortunately, in the presence of $AgPF_6$, complex **2** cannot transform to the RuFe analogue of **5**, but fast decomposed into unknown insoluble species.

Subsequently, we examined the reactivity of complex **3** toward ligand exchange with sodium azide (NaN_3). Treatment of **3** with NaN_3 in acetonitrile at room temperature gave an iron-cobalt azido complex $[Cp^*Co(MeCN)N_2S_2Fe(N_3)][PF_6]$ (**6**) in a moderate yield, which is different from the reaction of zero-valent iron species with organic azide to give an imido complex [44]. The ESI-HRMS of **6** shows an expected molecular ion peak at *m/z* 498.0856 (calcd. 498.0859) for $[\mathbf{6}-MeCN-PF_6]^+$. Similarly, the ^{1}H NMR spectroscopic analysis of **6** also displays a characteristic broad signal at δ 0.51 ppm, which suggests **6** should also be a paramagnetic species. In the IR spectrum of **6**, a very strong absorption band at 2069 cm^{-1} is attributed to the stretching vibration of azide, which is very close to those of sulfide- or thiolate-bridged iron-containing complexes with the azido ligand in an end-on terminally coordinated fashion [45,46]. In order to obtain the single-crystals suitable for X-ray diffraction analysis, we performed the facile counterion exchange reaction of **6** with $NaBPh_4$ at room temperature to afford an analogous complex $[Cp^*Co(MeCN)N_2S_2Fe(N_3)][BPh_4]$ (**6′**).

The solid-state structure of **6′** was confirmed by single-crystal X-ray diffraction analysis (Fig. 3b). The Fe–N3 bond length of 1.993(4) Å in **6′** is obviously longer than those of some mono-iron azido complexes (1.859(5)–1.934(7) Å) [45,47,48]. Unexpectedly, complex **2** cannot react with NaN_3 even under heating. These experimental results demonstrated that another different metal could be an important factor to the reactivity of the $\{N_2S_2FeCl\}$ moiety.

One step further, we also explored the catalytic hydrazine disproportionation to ammonia using **2, 3** and **4** as catalysts. Treat-

Table 2
Catalytic disproportionation of hydrazine by **2, 3** and **4**.[a]

$$3\ N_2H_4 \xrightarrow[MeCN,\ r.t.\ \ 12\ h]{Cat.\ (5\ mol\%)} 4\ NH_3 + N_2$$

Entry	Catalyst	NH_3 yield (%)[b]
1	$[Cp^*Ru(MeCN)N_2S_2FeCl][PF_6]$ (**2**)	35
2	$[Cp^*Co(MeCN)N_2S_2FeCl][PF_6]$ (**3**)	5
3	$[Cp^*CoN_2S_2FeCl]$ (**4**)	trace

[a] N_2H_4 (0.4 mmol), catalyst (5 mol%), CH_3CN (5 mL), r.t., 12 h.
[b] The resulted NH_3 was converted into NH_4Cl by mixing with $HCl{\cdot}Et_2O$. The yields of NH_4Cl were quantified by integration of the NH_4^+ resonance with respect to an internal reference of ferrocene in NMR.

ment of a CH_3CN solution of **2** with 20 equiv. of hydrazine at room temperature afforded ammonia in 35% yield (Table 2, entry 1), which is comparable to other thiolate-bridged RuFe complexes [37]. Reaction of **3** with hydrazine was also performed under the same conditions and ammonia was obtained in 5% yield (Table 2, entry 2), which reveals that complex **3** can only convert hydrazine to ammonia stoichiometrically. In addition, complex **4** exhibited no catalytic activity towards hydrazine disproportionation and only a trace amount of ammonia was detected (Table 2, entry 3). Given that the initial electrons for N−N bond cleavage of hydrazine are provided by the complex itself, we speculate that the obviously different performance in converting the hydrazine to ammonia between the RuFe and CoFe complexes is likely attributed to the stability under oxidation, which is consistent with the results of electrochemical studies.

In conclusion, we synthesized and characterized two iron-cobalt and iron-ruthenium complexes with the same coordination sphere as the diiron complex $[Cp^*Fe(MeCN)N_2S_2FeCl][PF_6]$. The electrochemical and DFT analyses of the two heterobinuclear complexes suggested the redox properties and spin distributions of the $\{N_2S_2FeCl\}$ moiety were obviously affected by another metallic center. When reacting with reducing agent in CH_2Cl_2, CoFe complex can keep its integral framework without decomposing, compared with its FeFe and RuFe analogues. Furthermore, only CoFe complex can accomplish the ligand exchange reaction of the labile chloride with inorganic salts such as $AgPF_6$ or NaN_3. In addition, RuFe complex shows better catalytic reactivity toward the disproportionation of hydrazine into ammonia. Further studies on the design and synthesis of new heterobinuclear complexes and their catalytic properties are underway.

Declaration of competing interest

The authors declare no competing financial interests.

Acknowledgments

This work was supported by the National Natural Science Foundation of China (Nos. 21690064, 22001031), the key laboratory of Bio-based Chemicals of Liaoning Province of China, the "111" project of the Ministry of Education of China and the Fundamental Research Funds for the Central Universities (No. DUT19RC(3)013).

Supplementary materials

Supplementary material associated with this article can be found, in the online version, at doi:10.1016/j.cclet.2021.06.070.

References

[1] J.C. Fontecilla-Camps, P. Amara, C. Cavazza, et al., Nature 460 (2009) 814–822.
[2] W. Lubitz, H. Ogata, O. Rüdiger, et al., Chem. Rev. 114 (2014) 4081–4148.
[3] P.A. Lindahl, J. Inorg. Biochem. 106 (2012) 172–178.
[4] X. Wang, Z. Wang, T.T. Zhuang, et al., Nat. Commun. 10 (2019) 5186.
[5] S. Ogo, K. Ichikawa, T. Kishima, et al., Science 339 (2013) 682–684.
[6] K. Tanifuji, Y. Ohki, Chem. Rev. 120 (2020) 5194–5251.
[7] P. Buchwalter, J. Rosé, P. Braunstein, Chem. Rev. 115 (2015) 28–126.
[8] D.R. Pye, N.P. Mankad, Chem. Sci. 8 (2017) 1705–1718.
[9] L. Hao, J. Xiao, J.J. Vittal, et al., Organometallics 16 (1997) 2165–2174.
[10] S.H. Druker, M.D. Curtis, J. Am. Chem. Soc. 117 (1995) 6366–6367.
[11] V. Ritleng, M.J. Chetcuti, Chem. Rev. 107 (2007) 797–858.
[12] M. Melnik, J. Garaj, C.E. Holloway, J. Coord. Chem. 61 (2008) 3021–3065.
[13] S. Maggini, Coord. Chem. Rev. 253 (2009) 1793–1832.
[14] S. Sculfort, P. Braunstein, Chem. Soc. Rev. 40 (2011) 2741–2760.
[15] Y. Ishii, K. Miyashita, K. Kamita, et al., J. Am. Chem. Soc. 119 (1997) 6448–6449.
[16] N. Yoshikai, M. Yamanaka, I. Ojima, et al., Organometallics 25 (2006) 3867–3875.
[17] C.M. Farley, C. Uyeda, Trends Chem. 1 (2019) 497–509.
[18] J. Campos, Nat. Rev. Chem. 4 (2020) 696–702.
[19] G. Liu, P. Poths, X. Zhang, et al., J. Am. Chem. Soc. 142 (2020) 7930–7936.
[20] S. Komiya, Coord. Chem. Rev. 256 (2012) 556–573.
[21] M. Clemente-León, E. Coronado, C. Martí-Gastaldo, et al., Chem. Soc. Rev. 40 (2011) 473–497.
[22] Y. Chen, Y. Zhou, P. Chen, et al., J. Am. Chem. Soc. 130 (2008) 15250–15251.
[23] Y. Chen, L. Liu, Y. Peng, et al., J. Am. Chem. Soc. 133 (2011) 1147–1149.
[24] Y. Li, Y. Li, B. Wang, et al., Nature Chem. 5 (2013) 320–326.
[25] D. Yang, Y. Li, L. Su, et al., Eur. J. Inorg. Chem. 2015 (2015) 2965–2973.
[26] P. Sun, D. Yang, Y. Li, et al., Organometallics 35 (2016) 751–757.
[27] P. Tong, W. Xie, D. Yang, et al., Dalton Trans. 45 (2016) 18559–18565.
[28] Y. Zhang, D. Yang, Y. Li, et al., Dalton Trans. 46 (2017) 7030–7038.
[29] Q. You, D. Yang, S. Xu, et al., Inorg. Chem. Commun. 106 (2019) 27–33.
[30] K.D. Karlin, S.J. Lippard, J. Am. Chem. Soc. 98 (1976) 6951–6957.
[31] L. Su, D. Yang, Y. Zhang, et al., Chem. Commun. 54 (2018) 13119–13122.
[32] P.J. Fagan, M.D. Ward, J.C. Calabrese, J. Am. Chem. Soc. 111 (1989) 1698–1719.
[33] G. Fairhurst, C. White, J. Chem. Soc., Dalton Trans. (1979) 1524–1530.
[34] S. Venkataramani, U. Jana, M. Dommaschk, et al., Science 331 (2011) 445–448.
[35] M. Yuki, Y. Miyake, Y. Nishibayashi, Organometallics 29 (2010) 5994–6001.
[36] D. Yang, Y. Li, B. Wang, et al., Inorg. Chem. 54 (2015) 10243–10249.
[37] Y. Zhang, J. Zhao, D. Yang, et al., Inorg. Chem. Commun. 83 (2017) 66–69.
[38] Y. Zhang, D. Yang, Y. Li, et al., Catal. Sci. Technol. 9 (2019) 6492–6502.
[39] S. Cai, X.F. Hou, Y.Q. Chen, et al., Dalton Trans. (2006) 3736–3741.
[40] H. Gao, J. Huang, L. Chen, et al., RSC Adv. 3 (2013) 3557–3565.
[41] P. Ghosh, M. Quiroz, N. Wang, et al., Dalton Trans. 46 (2017) 5617–5624.
[42] C.Y. Chiang, J. Lee, C. Dalrymple, et al., Inorg. Chem. 44 (2005) 9007–9016.
[43] S. Ding, P. Ghosh, A.M. Lunsford, et al., J. Am. Chem. Soc. 138 (2016) 12920–12927.
[44] W. Chen, Q. Chen, Y. Ma, et al., Chin. Chem. Lett. 31 (2020) 1342–1344.
[45] Y. Zhang, T. Mei, D. Yang, et al., Dalton Trans. 46 (2017) 15888–15896.
[46] E. Dumas, J. Marrot, J. Jullien, et al., Inorg. Chim. Acta 358 (2005) 70–76.
[47] C.A. Grapperhaus, B. Mienert, E. Bill, et al., Inorg. Chem. 39 (2000) 5306–5317.
[48] G. Sabenya, L. Lázaro, I. Gamba, et al., J. Am. Chem. Soc. 139 (2017) 9168–9177.